MoMI-G: Modular Multi-scale Integrated Genome Graph Browser

Toshiyuki T. Yokoyama, Yoshitaka Sakamoto, Masahide Seki, Yutaka Suzuki, Masahiro Kasahara*

Affiliations

Department of Computational Biology and Medical Sciences, Graduate School of Frontier Sciences,

The University of Tokyo, Chiba, Japan

*Correspondence should be addressed to

Masahiro Kasahara

E-mail: mkasa@k.u-tokyo.ac.jp

Tel/Fax: +81 4 7136 4110

ABSTRACT

Genome graph is an emerging approach for representing structural variants on genomes with branches. For example, representing structural variants of cancer genomes as a genome graph is more natural than representing such genomes as differences from the reference genome. However, there is currently no visualization method for large genome graphs, such as human cancer genomes. To this end, we developed MOdular Multi-scale Integrated Genome graph browser, MoMI-G, a web-based genome graph browser that can visualize genome graphs with structural variants and supporting evidences such as read alignments, read depth, and annotations.

KEYWORDS

Structural Variant; Genome Graphs; Genome Browser; Visualization; Variation Graphs; Long-read Sequencing;

INTRODUCTION

Structural Variants (SVs), which are often characterized as 50 bp or larger genomic rearrangements of chromosomal segments, are associated with various human diseases [1–3]. For example, some fusion genes caused by SVs are known oncogenes [4]. Identifying SVs and interpreting their potential impacts are critical steps toward cataloguing the variations in the human genome and mechanistic understanding of genetic diseases and cancers.

SV visualization is a very important step in an SV calling process, because it enables the manual inspection of SVs for achieving two goals: The first is to better understand the relationships between SVs and other genomic features, and the second is to ensure a smaller number of false positives.

For the first goal, SV visualization tools should be able to simultaneously display multiple intervals along with their relationships, even when the breakpoints are distant or when SVs are nested. Older SV visualization tools focus on visualizing only canonical SVs (insertion, deletion, inversion, duplication, and translocation) [5,6], because they account for a significant portion of the identified SVs at that time. However, as long-read sequencing technologies reveal an increasing number of SVs, SV visualization with the existing tools becomes more challenging. For example, a large inversion is often identified as two separate translocations at the two breakpoints of the inversion; one might not be able to immediately recognize that the two translocation events are explained by a single large inversion. Another example is a nested SV. When there is a large inversion that contains several smaller SVs, such as insertion of transposons or deletions, the nested SVs often obscure the relationship between genomic regions that are distant in the reference genome, but are actually close in the target genome. To this end, we employed genome graphs as a theoretical backbone for providing more systematic way of presenting SVs with varying complexities, including nested and large SVs [7]. Genome graphs can represent SVs more naturally than those that represent SVs as differences from a

52 reference genome (e.g., VCF). However, there is no visualization method for large genome graphs,
53 such as human cancer genomes.

54 For the second goal, manual inspection of SVs identified using SV calling tools is important,
55 because these tools are not yet accurate enough; human experts are required to accurately and reliably
56 distinguish true positive SVs from false positive ones. For example, SVs identified by using reads
57 obtained by different sequencing platforms are often not concordant [8], suggesting that the algorithms
58 of SV callers need further improvement. Therefore, SV candidates need to be manually inspected using
59 read alignments and genomic annotations [9]. Developers of SV callers may wish to track down false
60 positives, so they can improve the algorithms. Biologists may wish to filter out false positives through
61 manual inspection to find genuine causal SVs. However, manual inspection by using existing SV
62 visualization tools occasionally becomes very difficult for certain cases. For example, for nested SVs
63 and long reads spanning over multiple breakpoints, existing tools cannot show the read alignments in
64 multiple intervals at a glance, making it unrealistic to manually judge the authenticity of candidate
65 SVs. Another example is that tandem duplications identified by SV callers are often inaccurate. This
66 is presumably because the accuracy for finding tandem duplications has not been optimized for real
67 biological data [8,10,11].

68 To achieve these two goals, we developed MoMI-G (pronounced mo-me-jee), a genome
69 graph browser that visualizes SVs using variation graphs (Fig. 1, Additional file 1: Supplemental Fig.
70 1), a variant of genome graphs [12]. Herein, we describe the use cases and features of MoMI-G using
71 the LC-2/ad human lung adenocarcinoma cell line that carries a CCDC6-RET fusion gene [13–16],
72 and CHM1, a human hydatidiform mole cell line that originates from a single haploid [17]. MoMI-G
73 helps in understanding the entire picture of SVs, even those that are nested or large, regardless of their
74 size. MoMI-G allows researchers to obtain novel biological knowledge by comparing a reference
75 genome with an individual genome by using a variation graph.

A.

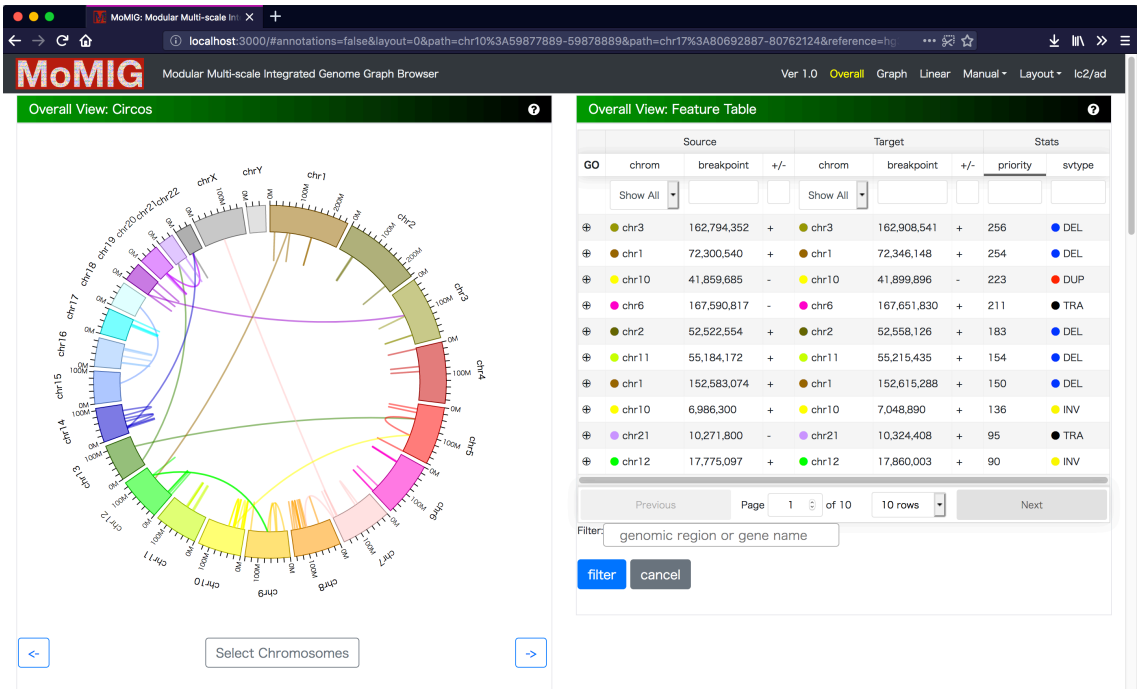
MoMIG: Modular Multi-scale Integ
localhost:3000/#annotations=false&layout=0&path=chr10%3A59877889-59878889&path=chr17%3A80692887-80762124&reference=hg
MoMIG
Modular Multi-scale Integrated Genome Graph Browser
Ver 1.0
Overall
Graph
Linear
Manual
Layout
lc2/ad
Overall View: Circos
Overall View: Feature Table
Source
Target
Stats
GO
chrom
breakpoint
+/-
chrom
breakpoint
+/-
priority
svtype
Show All
Show All
chr3 162,794,352 + chr3 162,908,541 + 256 DEL
chr1 72,300,540 + chr1 72,346,148 + 254 DEL
chr10 41,859,685 - chr10 41,899,896 - 223 DUP
chr6 167,590,817 - chr6 167,651,830 + 211 TRA
chr2 52,522,554 + chr2 52,558,126 + 183 DEL
chr11 55,184,172 + chr11 55,215,435 + 154 DEL
chr1 152,583,074 + chr1 152,615,288 + 150 DEL
chr10 6,986,300 + chr10 7,048,890 + 136 INV
chr21 10,271,800 - chr21 10,324,408 + 95 TRA
chr12 17,775,097 + chr12 17,860,003 + 90 INV
Previous
Page 1 of 10
10 rows
Next
Filter:
genomic region or gene name
filter
cancel
Select Chromosomes

B.

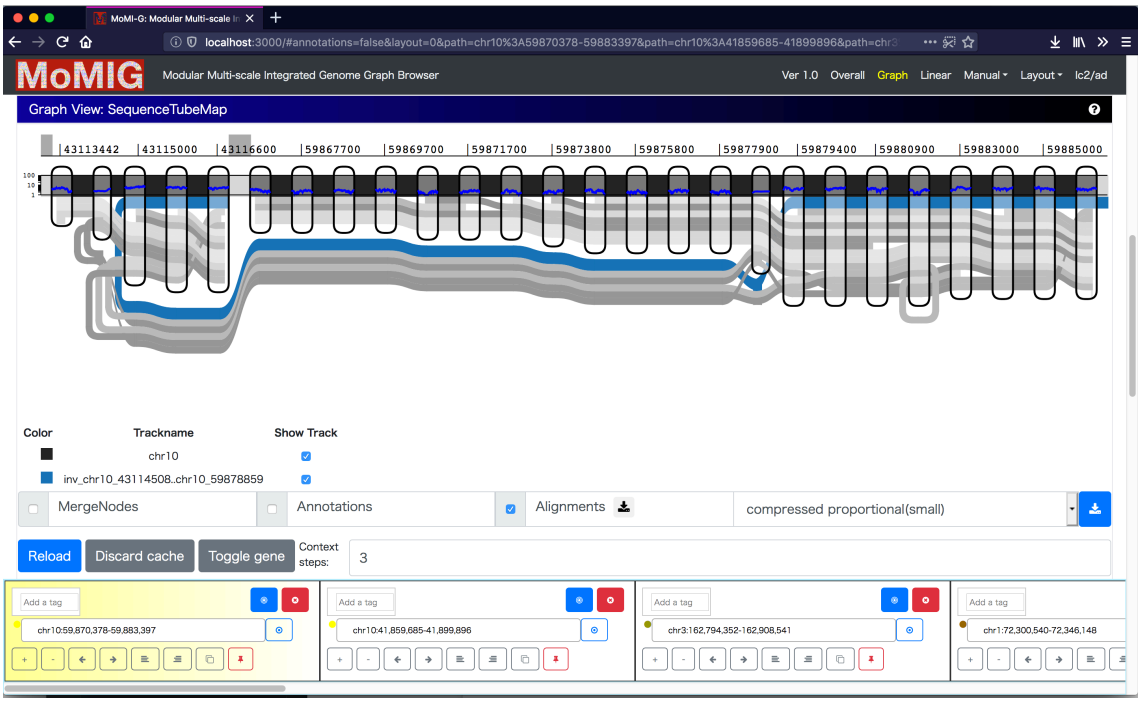
MoMI-G: Modular Multi-scale Integ
localhost:3000/#annotations=false&layout=0&path=chr10%3A59870378-59883397&path=chr10%3A41859685-41899896&path=chr3
MoMIG
Modular Multi-scale Integrated Genome Graph Browser
Ver 1.0
Overall
Graph
Linear
Manual
Layout
lc2/ad
Graph View: SequenceTubeMap
43113442
43115000
43116600
59867700
59869700
59871700
59873800
59875800
59877900
59879400
59880900
59883000
59885000
Color
Trackname
Show Track
chr10
inv_chr10_43114508..chr10_59878859
MergeNodes
Annotations
Alignments
compressed proportional(small)
Reload
Discard cache
Toggle gene
Context steps:
3
Add a tag
chr10:59,870,378-59,883,397
Add a tag
chr10:41,859,685-41,899,896
Add a tag
chr3:162,794,352-162,908,541
Add a tag
chr1:72,300,540-72,346,148

C.

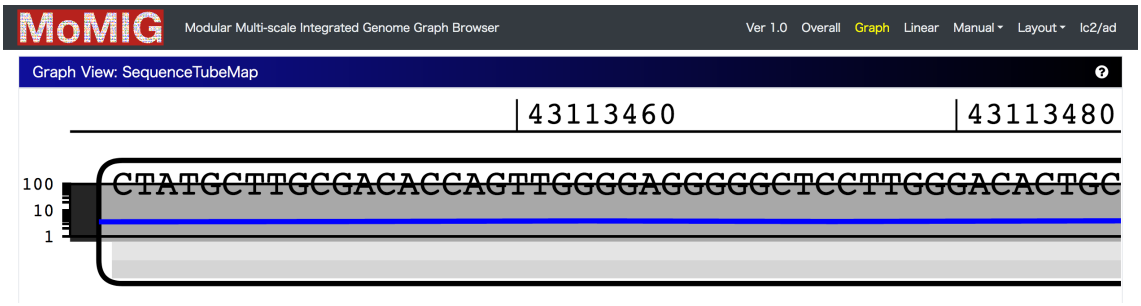

Figure 1. Overview of MoMI-G. A user typically selects one of the preset combinations of view modules. The user can customize the window by adding or removing view modules, if necessary. Three examples showing views of different scales are shown. Comprehensive descriptions for all modules are shown in Additional file 1: Supplemental Fig. 1.

(A) Chromosome-scale view: Circos Plot (left) shows the distribution of SVs over all chromosomes. Arcs are chromosomes. Curves represent SVs. Feature Table (right) shows a filtered/sorted list of the SVs in an input VCF file.

(B) Gene-scale view: SequenceTubeMap (top) shows the graphical view of the genomic region selected in Circos Plot, Feature Table, or Interval Card Deck. A rounded rectangle is a node that represents a piece of a genomic sequence. The thick lines spanning over nodes are paths; the horizontal thick black line with light/dark shades is a chromosome of the reference genome, and the blue line indicates one end of an inversion. The color of lines indicating SVs is assigned arbitrarily. Read alignments are shown as gray thin lines, suggesting that the inversion here is likely heterozygous. Interval Card Deck (bottom) queues a list of genomic intervals for candidate SVs selected by using Circos Plot or Feature Table for rapidly screening hundreds of candidate intervals.

(C) Nucleotide-scale view: SequenceTubeMap can show nucleotides.

RESULTS

MoMI-G is a web-based genome browser developed as a single-page application implemented in TypeScript and with React. Because users need different types of views, even for the same data, MoMI-G provides three groups of view modules for the analysis of SVs at different scales, namely chromosome-scale, gene-scale, and nucleotide-scale view groups (Additional file 1: Supplemental Table 1). Users can use one or more view modules in a single window.

The input of MoMI-G is a variation graph, read alignment (optional), and annotations (optional). MoMI-G accepts a succinct representation of a vg variation graph, which is an XG file, as a variation graph. A script that converts a FASTA file of a reference genome and a common variant format (VCF) file into an XG file is included in the MoMI-G package, although the VCF format cannot represent some types of SVs that the XG format can represent, such as nested insertions. Read alignment data on the graph need to be represented as a graph alignment map (GAM) file; alternatively, users can convert a binary alignment map (BAM) file into a GAM file, although this is not recommended due to some limitations.

We show three examples from two samples to demonstrate the utility of MoMI-G. One of the examples is a large inversion, and the other is nested SVs that are difficult to visualize using existing tools. We also show nested SVs from the CHM1 dataset [17]. For all the examples, we used the Amazon EC2 instance type t2.large with 8 GB of memory and 2.4 GHz Intel Xeon processor as the MoMI-G server; the server requirement for this tool is minimal. MoMI-G supports common browsers, including Chrome, Safari, and Firefox.

Data model used in MoMI-G and MoMI-G tools

To our knowledge, no publicly available SV visualization tools are available for large and nested SVs

126 with alignments of long reads. Thus, we aimed to develop a genome graph browser at the earliest so
127 that users can obtain new biological knowledge from real data. We used an existing library,
128 SequenceTubeMap (https://github.com/vgteam/sequenceTubeMap), for visualizing a variation
129 subgraph, rather than developing our own library from scratch.

130 SequenceTubeMap is a JavaScript library that visualizes multiple related sequences such as
131 haplotypes. A variation graph used in SequenceTubeMap is a set of nodes and paths, where a node
132 represents part of a DNA sequence, and a path represents (part of) a haplotype. Edges are implicitly
133 represented by adjacent nodes in paths.

134 MoMI-G accepts variation graphs in which SVs are represented by paths so that
135 SequenceTubeMap can visualize them. A deletion is represented by a path that skips over a sequence
136 that other paths pass through. Similarly, an insertion is represented by a path that passes through an
137 extra sequence that other paths do not visit; an inversion is represented by a path where part of the
138 sequence in other paths is reversed; and, a duplication is represented by a path that passes through the
139 same sequence twice or more.

140 The MoMI-G package includes a set of scripts (MoMI-G tools) that convert a VCF file into
141 the variation graph format. We used MoMI-G tools for generating the input variation graphs;
142 alternatively, users can generate variation graphs on their own. See the method section and Additional
143 file 1: Supplemental Figure 2 for details of the MoMI-G tools. Briefly, MoMI-G tools convert a VCF
144 record into a path in the output variation graph. A deletion is converted into a path that starts, at most,
145 1 Mbp before one breakend of the deletion, traverses to the breakend, jumps to the other breakend,
146 and proceeds for a certain length (<1 Mbp). Note that the sequences flanking the deletion are added to
147 indicate the edge representing the deletion because edges are implicitly represented in
148 SequenceTubeMap. Insertions, inversions, and duplications are similarly represented by paths with
149 flanking sequences.

150

151 **Visualization Examples**

152 *Revealing a large SV: A large inversion and a subsequent short deletion*

153 Using MoMI-G, we show an example of a complex SV that involves two SVs identified by Sniffles,
154 each of which connects two different points on a chromosome. This complex SV can be considered a
155 large inversion and two flanking deletions. Previous studies involving the use of whole genome
156 sequencing or RNA-seq with the Illumina HiSeq or Nanopore MinION identified the CCDC6-RET
157 fusion gene in LC-2/ad [14–16,18]. However, those studies focused only on the region around the
158 CCDC6-RET fusion point, and the entire picture, including the other end of the inversion, was unclear.
159 To address this issue, we explored the wider region around CCDC6-RET with MoMI-G.

160 First, we sequenced the genome of LC-2/ad with Oxford Nanopore MinION R9.5 pore
161 chemistry and merged reads with those from a previous study (accession No. DRX143541-
162 DRX143544) [18]. We generated 3.5 M reads to 12.8× coverage in total and then aligned them with
163 GRCh38. The average length of the aligned reads was 16 kb (Additional file 1: Supplemental Table
164 2). We detected 11,316 SVs in the VCF format, including the previously known CCDC6-RET fusion
165 gene, on the nuclear DNA of LC-2/ad cell line (Additional file 1: Supplemental Table 3). See the
166 methods section for details.

167 The distance between RET (chr10: 43,075,069–43,132,349) and CCDC6 (chr10:
168 59,786,748–59,908,656) is about 17 Mbp in GRCh38. We confirmed that a CCDC6-RET fusion gene
169 exists in LC-2/ad (Fig. 2A). This fusion gene is presumably caused by an inversion, although only one
170 end of the inversion was found. We found an unknown novel adjacency that well explains the other
171 end of the inversion (Fig. 2B, Additional file 1: Supplemental Table 4). MoMI-G was able to display
172 the relationships between the two breakends of the inversion, enabling users to understand large SVs.
173 We explored the read alignments around the fusion and found that the fusion was heterozygous (Fig.

174 2C). MoMI-G is the first stand-alone genome graph browser that can display long-read alignments
175 over branching sequences that represent a heterozygous SV.

176 Further, we found that the large inversion was flanked by two small deletions. These
177 deletions are explained by a single deletion event following the large inversion event (Fig. 2D). The
178 loss of the RET-CCDC6 fusion gene corresponds to the two small deletions on GRCh38. A simple
179 explanation is that a deletion occurred after the inversion event, but not vice versa, in favor of the
180 smaller number of mutation events.

181 Next, we attempted to estimate the breakpoints of the large inversion before the deletion
182 occurred. There were two possible scenarios for the positions of the two breakends of the large
183 inversion. The first is that RET-CCDC6 and CCDC6-RET were generated by a large inversion and
184 then RET-CCDC6 was lost. The second is that CCDC6 was first broken by a large inversion, and a
185 subsequent small deletion led to CCDC6-RET. Previous studies support the former scenario. First, the
186 RET gene often tends to be disrupted in thyroid cancer by paracentric inversion of the long arm of
187 chromosome 10, or by chromosomal fusion [19]. Second, in a previous study, two clinical samples
188 had both RET-CCDC6 and CCDC6-RET in the genome [20]. Both studies suggested that an inversion
189 disrupted both CCDC6 and RET, and then a small deletion disrupted RET-CCDC6. We could never
190 recognize these two deletions flanking the large inversion without simultaneously observing both the
191 inversion records in VCF.
192

193 *Nested SVs with alignment coverage*

194 Visualizing nested SVs is necessary for evaluating the output of SV callers. However, most existing
195 genome browsers cannot visualize nested SVs as well as the relationships between them. Genome
196 browsers, including IGV [21], collapse SVs into intervals between breakpoints, and thus the

197 topological relationships between nested SVs are not shown. MoMI-G can visualize nested SVs as a
198 variation graph (Fig. 3).
199
200 *Visualizing nested SVs in a pseudodiploid genome*
201 We show an example of nested SVs in a pseudodiploid genome visualized using MoMI-G. We
202 downloaded a CHM1 genome with an SV list previously generated in a whole-genome resequencing
203 study with PacBio sequencers from human hydatidiform [17]. The SV list includes insertions,
204 deletions, and inversions for GRCh37/hg19. We converted the BED file of the SV list of CHM1 to a
205 VCF file, and then filtered out deletions of less than 1,000 bp to focus on medium to large SVs. We
206 found nested SVs for which existing genome browsers do not intuitively show the relationships
207 between them (Fig. 4). This example indicates that four insertions and deletions occur in the large
208 inversion.
209
210 **A.**

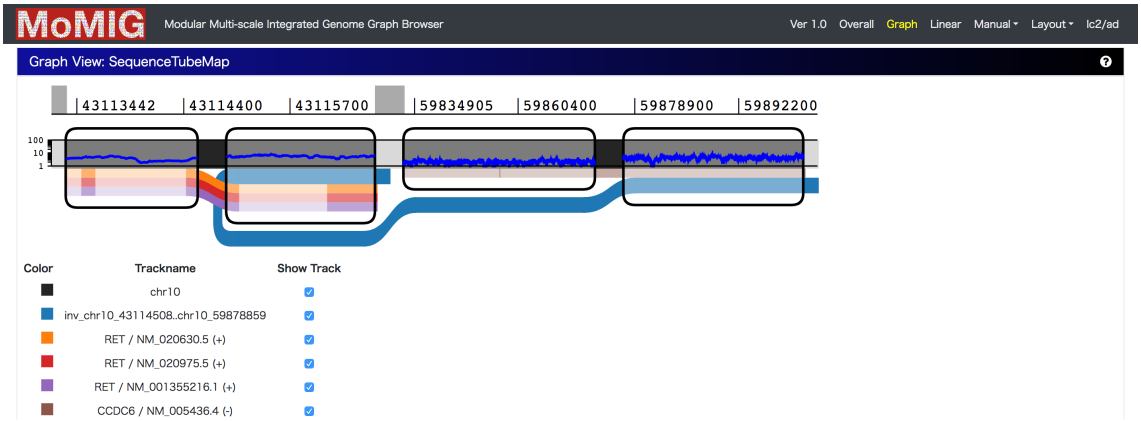

211
212
213 **B.**
214

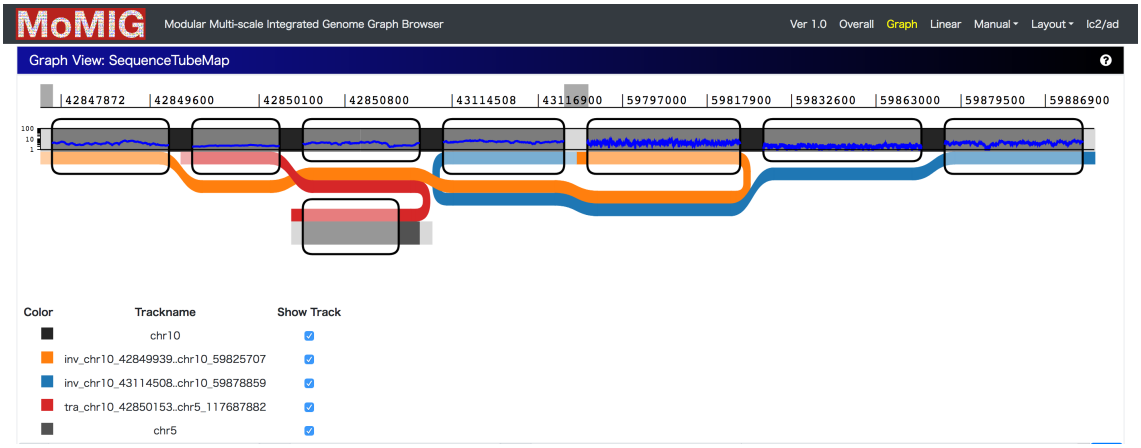

215

216

217 **C.**

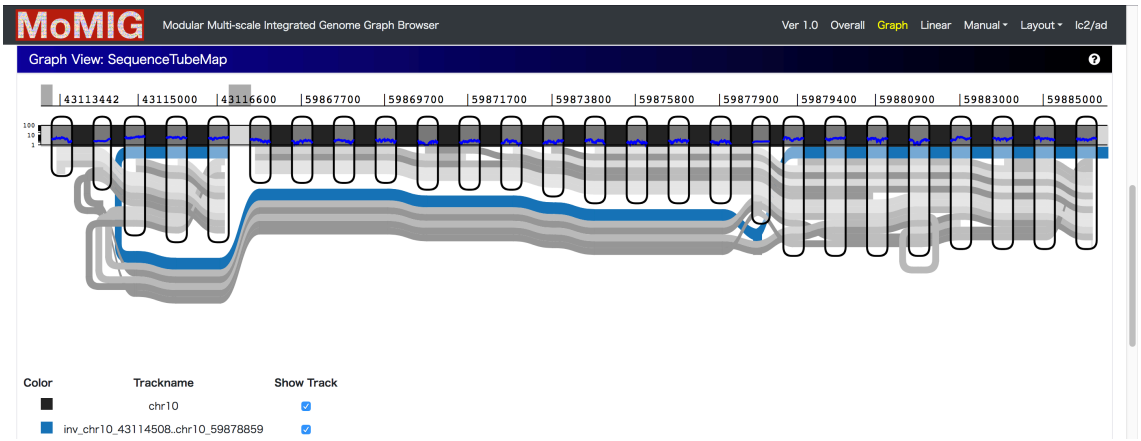

218

219

220 **D.**

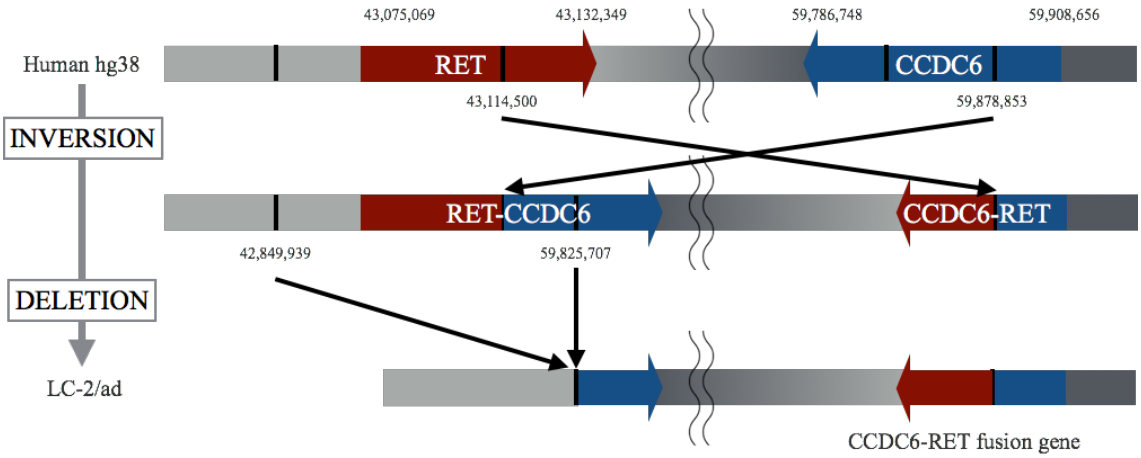

221

Figure 2. Example of CCDC6-RET

(A) CCDC6-RET shown in MoMI-G (compressed view). The thickest black line is chromosome 10 (reference genome). Note that the two distinct intervals of chromosome 10 are shown, which correspond to the RET (left interval) and CCDC6 (right interval) genes. The blue line represents an inversion identified by Sniffles, showing the CCDC6-RET fusion event. The other lines are gene annotations in hg38; the orange, red, and purple lines indicate two isoforms of RET, and the brown line is CCDC6. (B) CCDC6-RET with read alignments shown as grey lines. Further, some alignments do not support the inversion, suggesting that CCDC6-RET is heterozygous. (C) The entire picture of the inversion that caused CCDC6-RET. This inversion is too large to span by a single read; thus, it was identified as two independent fusion events at both the ends of the inversion, which would be difficult to understand if the two fusion events are visualized separately. The red line is a translocation that was not analyzed in this study. (D) Putative evolution process of LC-2/ad at the CCDC6-RET site. First, a long inversion generated two fusion genes, CCDC6-RET and RET-CCDC6. Second, a large deletion caused the loss of RET-CCDC6.

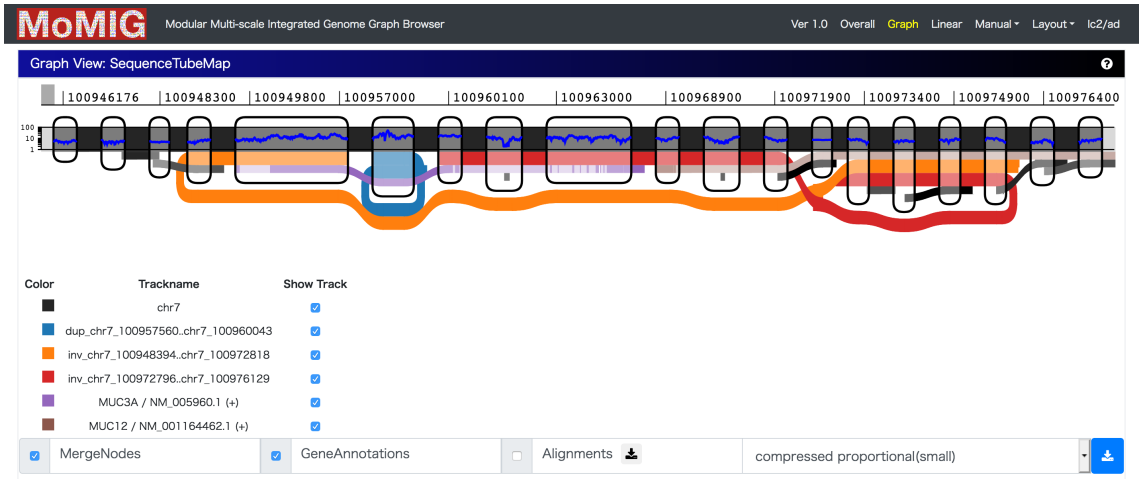

Figure 3. Nested SVs called by Sniffles in LC-2/ad

The thin black lines are repeat annotations. The brown and purple lines are gene annotations. The red and orange lines are an end of an inversion called by Sniffles. There are two possibilities for the genome structure: one is that MUC3A and its flanking region are a duplication, and the internal region of MUC12 is an inverted duplication. The other is that MUC3A and its flanking region are an inverted duplication, and the internal region of MUC12 is a duplication. Several read alignments support the former interpretation. Although SVs called from the Illumina reads did not include any of the SVs shown here, the alignment coverage by the Illumina reads is consistent with both duplications. Note that the y-axis of the blue thin line on the chromosome showing the alignment coverage is logarithmic.

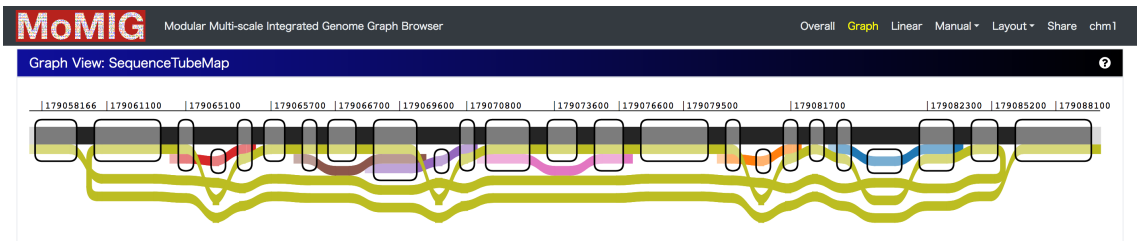

Figure 4. Nested SVs in CHM1

The black line represents a part of chromosome 5, where a large inversion is shown as the brown line. The other lines are smaller SVs included in the large inversion. Because CHM1 is a pseudodiploid genome, all the SVs shown in this figure must be on the same haplotype, although MoMI-G tools assume diploid (polyploid) genomes and show the inner SVs as heterozygous SVs.

User-interface Design

The optimal way of visualizing SVs might vary. To rapidly explore the distribution of SVs in a genome, users might wish to use Circos-like plots. Other users might intend to focus on local graph structures of SVs that contain a few genes. In another scenario, a user might want to explore individual nucleotides. To address this issue, MoMI-G provides a customizable view in which users can place any combination of view modules. Further, preset view layouts are available for users' convenience.

262

263 *Enabling easy manual inspection of detected SVs*

264 Manual inspection, which includes determining if an SV is heterozygous or homozygous, confirming
265 what part of a gene is affected by that SV, and determining the reason why an SV is called based on
266 read alignments, is an important part of validating called SVs. As variants called by SV callers increase,
267 the burden of manual inspection also increases, underscoring the importance of visualization both to
268 inspect individual SV calls for filtering out false positives and to ensure that a filtered set of SVs is of
269 high confidence [22,23]. MoMI-G helps with the efficient inspection of SVs by using (1) Feature Table,
270 which is an SV list, (2) Interval Card Deck, which is genomic coordinate stacks, and (3) shortcut keys.
271 The usage is as follows: (1) one can filter SVs using Feature Table, after which SVs are selected, and
272 then (2) the listed variants are stacked on Interval Card Deck at the bottom of the window. In Interval
273 Card Deck, intervals are displayed as cards, and the interval at the top (leftmost) card of the deck is
274 shown on SequenceTubeMap. Each card can be dragged, and the order of cards can be changed. If one
275 double-clicks on a card, the card moves to the top of the deck. A tag can be added for a card for later
276 reference. Further, a card can be locked to avoid unintended modification or disposal, and the gene
277 name can be input with autocompletion for specifying the interval of a card.

278 When the interval to view is changed, only part of the view that needs an update is re-
279 rendered, whereas most genome browsers working on web interface require rendering the entire view.
280 Interval Card Deck enables the rapid assessment of hundreds of intervals. Moreover, deciding whether
281 an SV should be discarded or held becomes easier with shortcut keys. After all SVs are inspected, a
282 set of SVs held on the Interval Card Deck is obtained, which might be a set of interesting SVs or a set
283 of manually validated SVs. MoMI-G enables the rapid inspection of hundreds of SVs, providing a tool
284 for validating hundreds of SVs or for selecting interesting SVs.

285

286 *Input requirements*

287 MoMI-G inputs an XG format as a variation graph. Users can specify a GAM file with an index that

288 contains read alignment. They can convert a BAM file into GAM using MoMI-G tools or can generate
289 the GAM file on their own. When a BED file of genes is provided, users can specify a genomic interval
290 by gene name. A configuration file is written in YAML. MoMI-G also accepts bigBed and bigWig
291 formats [24] for visualizing annotations (e.g., repeats, genes, alignment depth, and GC content) on the
292 reference genome. The bigBed and bigWig need to be extended for genome graphs in the future. The
293 list of formats that are accepted by MoMI-G is shown in Table 1.
294
295 **Table 1. MoMI-G data files**
296

File type	Extension	Description
A succinct index of variation graphs	.xg	Variation graphs displayed in MoMI-G.
Graphical alignment/map	.gam	Read alignment. (optional)
Comma-separated values	.csv	SV list for chromosome-scale view. (optional)
Browser extensible data	.bed	Used for converting gene names to genomic intervals. Also used for autocompletion of gene names. (optional)
Compressed binary indexed BED	.bb	Annotations. (optional)
Compressed binary indexed wiggle	.bw	Annotations. (optional)

297
298
299 ## DISCUSSION
300 We developed a genome graph browser, MoMI-G, that visualizes SVs on a variation graph. Existing
301 visualization tools for SVs show either one SV at a time, or all SVs together; the former does not allow
302 the understanding of the relationships between SVs, whereas the latter is useless when the target

genome is very large and the whole variation graphs are too complicated to view in a single screen (i.e., the hairball problem). MoMI-G allows viewing only part of the genome, which resolves the hairball problem, while providing an intuitive view for multiple SVs, including large and nested SVs. Further, MoMI-G enables the manual inspection of complex SVs by providing integrated multiple view modules; users can filter SVs, validate them with read alignments, and interpret them with genomic annotations.

We used vg as a server-side library and SequenceTubeMap as a client-side library for subgraph retrieval and visualization of genome graphs, because to our knowledge, these are the only combinations that are publicly available. We found that significant amounts of engineering efforts are required for an even better user experience. For example, vg is a standalone command line application that exits immediately after the given query is processed; therefore, it does not have a function to keep the succinct index on memory for later use; every time only part of the genome is retrieved, the entire index of several gigabytes is loaded, which is unnecessary overhead. SequenceTubeMap displays inversions and duplications as loops; however, we found that new users occasionally find it difficult to recognize the connections between nodes. Visualizing SVs is still an open problem.

The currently available tools and formats for SV analysis have many problems. First, different SV callers output different VCF records even for the same SV. For example, depending on SV callers, an inversion with both boundaries identified at a base pair level is represented by one of the following: (1) a single inversion record, (2) two inversion records at both ends, (3) two breakend records at both ends, or (4) four breakend records at both ends (a variant of (3), but the records are duplicated for both the strands). Thus, developing a universal tool for variant graph construction is difficult. Second, certain types of nested SVs, such as an insertion within an insertion, are impossible to represent in a VCF file without tricks, although variant graphs can easily handle these SVs.

326 Therefore, generating a variation graph from a VCF file including SVs is not ideal. We need an SV
327 caller that directly outputs variation graphs.

328 Fostering the ecosystem around variation graphs is important for delivering their benefits to
329 end users, as noted in the ecosystem around the SAM/BAM formats that spurred development of
330 production-ready tools for end users. MoMI-G is the first step toward such a goal, because the
331 availability of tools ranging from upstream analysis, such as read alignment to visualization, is critical
332 for the entire ecosystem.

333 This is the one million genome era that requires rapid and memory-sufficient data structure
334 to allow alignments and store haplotype information. Because most parts of the genome are shared
335 between individuals, we need to focus on differences for reducing computation time and resources.
336 Therefore, genome graph is considered promising, especially for human variation analysis. Moreover,
337 new visualization methods as well as genome analysis methods are required. Genome graph browsers
338 should be able to handle even thousands of genomes in the near future. MoMI-G is a step forward for
339 visualizing genome graphs and could allow the development of new algorithms on genome graphs.

340

341 **METHODS**

342 *Datasets*

343 High-molecular-weight (HMW) gDNA was extracted from lung cancer cell line, LC-2/ad by using a
344 Smart DNA prep(a) kit (Analykjena). WGS data were produced from MinION 1D sequencing (SQK-
345 LSK108), MinION 1D^2 sequencing (SQK-LSK308), and MinION Rapid sequencing (SQK-
346 RAD003). For MinION 1D sequencing, 4 μg HMW gDNA was quantified using Tape Station. DNA
347 repair was performed using NEBNext FFPE DNA Repair Mix (M6630, NEB). End-prep was
348 performed using NEBNext Ultra II End Repair/dA-Tailing Module (E7546L, NEB). Adapter ligation
349 was performed using NEBNext Blunt/TA Ligase Master Mix (M0367L, NEB) and the Ligation

350 Sequencing Kit 1D (SQK-LSK108, Oxford Nanopore Technologies). Libraries were sequenced for 48
351 h with MinION (R9.5 chemistry, Oxford Nanopore Technologies). For MinION 1D^2 sequencing, the
352 protocol was the same as that for 1D excluding adapter ligation by using Ligation Sequencing Kit
353 1D^2 (SQK-LSK308, Oxford Nanopore Technologies). The library for MinION Rapid sequencing
354 was prepared according to Sequencing Kit Rapid (SQK-RAD003, Oxford Nanopore Technologies).
355

356 *Nanopore data alignment*

357 Nanopore WGS data were aligned against the GRCh38 human reference genome by using NGM-LR
358 with "-x ont" option (version 0.2.6) for calling SVs with Sniffles version 1.0.7 [8]. MinION 1D^2
359 sequencing can produce a 1D^2 read, which integrates the information of a read and its complementary
360 read into one read. MinION 1D^2 sequencing produces two types of fastq files, 1D and 1D^2; there
361 was some redundancy between 1D and 1D^2 reads. Therefore, redundant 1D reads were removed, and
362 only 1D^2 reads were used. Moreover, some redundant 1D^2 reads were found. These reads were
363 removed from 1D^2 files and used as 1D reads. The percentage of the primary aligned reads was
364 54.7% (Additional file 1: Supplemental Table 2). This is because we did not filter out reads excluding
365 1D-fail reads of Rapid sequencing for alignment.
366

367 *SV calling*

368 Sniffles (version 1.0.7) with a parameter "-s 5" was used to call SVs. The minimum number of
369 supporting reads was determined such that we could detect the known large deletion of CDKN2A [14],
370 but alignment bias for a reference genome reduces the call rate of insertions compared to that of
371 deletions [17,25]. We detected 11,316 records as a VCF file of SVs, including CCDC6-RET, on the
372 nuclear DNA of LC-2/ad cell line (Additional file 1: Supplemental Table 3). Illumina HiSeq 2000
373 Paired-end WGS data (DDBJ accession number, DRX015205) aligned against GRCh38 by using bwa

374 (version 7.15) [26] were used for calling SVs with Lumpy (version 0.2.13) [27], delly (version 0.7.7)
375 [28] and manta (version 1.0.3) [29]. The results of these SV callers are listed in Additional file 1:
376 Supplemental Table 5. The four lists of SV candidates detected using Sniffles, Lumpy, delly, and manta
377 were merged using SURVIVOR (version 1.0.0) [30] with "5 sv_lists 1000 1 1 0 0" option for clustering
378 SV candidates (Additional file 1: Supplemental Fig. 3). Further, we filtered the merged candidates
379 based on the following three criteria: (1) Remove SVs of 0 bp to 1 kbp in length to focus on large SVs,
380 (2) Remove all insertions and non-canonical SV types: INVDUP, DEL/INV, and DUP/INS (technically
381 unnecessary, but we aimed at cross-validating SV candidates from Illumina reads with which
382 insertions and non-canonical SV types are hard to call), and (3) Remove SVs overlapping with the
383 intervals of the 10X default blacklist
384 (https://github.com/10XGenomics/supernova/blob/master/tenkit/lib/python/tenkit/sv_data/10X_GRC
385 h38_no_alt_decoy/default_sv_blacklist.bed) for reducing false positives. After filtering, we obtained
386 1,790 SV records.
387
388 *Constructing a variation graph*
389 We constructed a variation graph, including a reference genome (GRCh38) and an individual genome
390 (either LC-2/ad or CHM1). We developed scripts that we call MoMI-G tools. MoMI-G tools follow
391 the procedure in SplitThreader Graph [31].
392
393 1. Extract a breakpoint list from a VCF file generated by Sniffles.
394 2. Construct an initial variation graph with each chromosome of the GRCh38 primary assembly as
395 a single node.
396 3. Split nodes every 1 Mbp due to the limitation in the implementation of vg used during the
397 development of MoMI-G; otherwise, vg aborted with an error. The latest version of vg does not

398 have this limitation.

399 4. For each breakpoint in the breakpoint list, split the node of the graph that contains the breakpoint

400 into two nodes at the breakpoint.

401 5. Create paths that represent the chromosomes in the reference genome.

402 6. Create paths that represent SVs, each of which corresponds to one record in the input VCF file.

403 Further, add a node to the graph when the type of SV is an insertion.

404

405 The representation of SVs varies between SV callers: the same SV can be described in different ways

406 in the current VCF format. Although vg has a "construct" subcommand that constructs a variation

407 graph from a pair of a reference genome and a VCF file, "vg construct" is incompatible with the output

408 of SV callers we know of for the following reason. For example, an INV record in VCF means either

409 a single inversion (both ends included) or only one end of the inversion, depending on the

410 implementation of SV callers. We wrote custom scripts, MoMI-G tools, for Sniffles.

411 In general, to display read alignments, we recommend aligning against a variation graph by

412 directly using "vg map" instead of converting read alignments against the linear reference genomes

413 into the GAM format. Nevertheless, we intended to inspect the results of Sniffles; therefore, we wrote

414 a custom script to convert alignments against the linear reference (BAM file) into a GAM file by using

415 "vg annotate," during which CIGAR is lost; "vg annotate" was originally designed for placing

416 annotations in BED/GFF files on paths on variation graphs and not for alignments. One possible

417 solution to this issue is making SV callers graph-aware.

418

419 *Inspection of SV candidates*

420 We modified and integrated SequenceTubeMap into MoMI-G so that it can visualize a variation graph

421 converted from SVs that shows the difference between a reference genome and an individual genome.

422 The modifications made to SequenceTubeMap are shown in Additional file 1: Supplemental Table 6.
423 One can click on the download button for downloading an SVG image generated by
424 SequenceTubeMap so that a vector image can be used for publication.
425
426 *Visualizing annotations*
427 Ideally, MoMI-G provides annotations on variation graphs. However, annotations available in public
428 databases are for the linear reference genome. MoMI-G can display annotations in the bigWig/bigBed
429 formats. In particular, for human reference genomes, GRCh19/hg37 and GRCh38/hg38, MoMI-G
430 provides an interface for retrieving Ensembl gene annotations from the Ensembl SPARQL endpoint
431 [32] via SPARQList REST API (https://github.com/dbcls/sparqlist). The orientation of genes is shown
432 in the legend of SequenceTubeMap. Further, if one clicks on a gene name, the website of the gene
433 information in TogoGenome [33] opens.
434
435 *Miscellaneous modules*
436 Threshold Filter: Threshold Filter has two use cases: First, one can toggle checkboxes to select whether
437 to show inter-chromosomal SVs and/or intra-chromosomal SVs; second, one can filter SVs with a
438 slider based on the custom priority (possibly given by SV callers) of each SV.
439 Annotation Table: Annotation Table shows all annotations that are displayed on the
440 SequenceTubeMap. Moreover, annotations can be downloaded as a BED file.
441 Linear Genome Browser: To provide a compatible view of a selected genomic region, we integrated
442 Pileup.js [34] into MoMI-G.
443
444 *Backend server*
445 The MoMI-G backend server caches subgraphs once a client requests a genomic interval on a path. It

then retrieves annotations from bigWig and bigBed with a range query and provides JSON API with which the client can make queries.

DECLARATIONS

Ethics approval and consent to participate

Not applicable.

Consent for publication

Not applicable.

Availability of data and materials

Newly obtained long-read sequencing data of LC-2/ad were deposited in the DDBJ with accession numbers DRA007941 (DRX156303-DRX156310). Datasets included in this article are also provided in the database, DBTSS/DBKERO [35]. The source code of MoMI-G is available at https://github.com/MoMI-G/MoMI-G/ under the MIT license. It is written in TypeScript and was tested on Linux and Mac operating systems. Further, we have included an example dataset and annotations as a Docker image.

Competing interests

The authors declare that they have no competing interests.

Funding

This work was supported in part by Information-technology Promotion Agency, Japan (IPA) and Exploratory IT Human Resources Project (The MITOU Program) in the fiscal year 2017 and in part by JSPS KAKENHI (Grant Number, 16H06279).

472 *Authors' contributions*

473 All authors were involved in study design; TY wrote all code of MoMI-G; Y. Sakamoto preformed
474 MinION sequencing and SV analysis on LC-2/ad; TY, Y. Sakamoto, and MK drafted the manuscript;
475 MS and Y. Suzuki supervised the sequencing analysis; and MK supervised the study. All authors read
476 and approved the final manuscript.

477

478 *Acknowledgements*

479 We thank all testers who provided testing and feedback for MoMI-G. We also thank Kazuyuki Shudo
480 at the Tokyo Institute of Technology and Toshiaki Katayama at the Database Center for Life Science
481 (DBCLS) of Research Organization of Information and Systems (ROIS), Japan, for their useful and
482 insightful discussions, Sarun Sereewattanawoot and Ayako Suzuki at the University of Tokyo for
483 initial contributions to Illumina read alignment.

484

485 **REFERENCES**

486 1. Stankiewicz P, Lupski JR. Structural Variation in the Human Genome and its Role in
487 Disease. Annu Rev Med. 2010;61:437–55.

488 2. Weischenfeldt J, Symmons O, Spitz F, Korbel JO. Phenotypic impact of genomic structural
489 variation: Insights from and for human disease. Nat. Rev. Genet. Nature Publishing Group;
490 2013;125–38.

491 3. Sedlazeck FJ, Lee H, Darby CA, Schatz MC. Piercing the dark matter: bioinformatics of
492 long-range sequencing and mapping. Nat Rev Genet. Springer US; 2018;19:329–46.

493 4. Mertens F, Johansson B, Fioretos T, Mitelman F. The emerging complexity of gene fusions
494 in cancer. Nat Rev Cancer. Nature Publishing Group; 2015;15:371–81.

495 5. Quinlan AR, Hall IM. Characterizing complex structural variation in germline and somatic

496 genomes. Trends Genet. Elsevier Ltd; 2012;28:43–53.
497 6. Collins RL, Brand H, Redin CE, Hanscom C, Antolik C, Stone MR, et al. Defining the
498 diverse spectrum of inversions, complex structural variation, and chromothripsis in the morbid
499 human genome. Genome Biol. Genome Biology; 2017;18:36.
500 7. Paten B, Novak AM, Eizenga JM, Garrison E. Genome graphs and the evolution of genome
501 inference. Genome Res. 2017;665–76.
502 8. Sedlazeck FJ, Rescheneder P, Smolka M, Fang H, Nattestad M, von Haeseler A, et al.
503 Accurate detection of complex structural variations using single-molecule sequencing. Nat
504 Methods. Springer US; 2018;15:461–8.
505 9. Guan P, Sung W-K. Structural variation detection using next-generation sequencing data.
506 Methods. Elsevier Inc.; 2016;102:36–49.
507 10. English AC, Salerno WJ, Reid JG. PBHoney: identifying genomic variants via long-read
508 discordance and interrupted mapping. BMC Bioinformatics. 2014;15:180.
509 11. Cretu Stancu M, van Roosmalen MJ, Renkens I, Nieboer MM, Middelkamp S, de Ligt J, et
510 al. Mapping and phasing of structural variation in patient genomes using nanopore sequencing.
511 Nat Commun. 2017;8:1326.
512 12. Garrison E, Sirén J, Novak AM, Hickey G, Eizenga JM, Dawson ET, et al. Variation graph
513 toolkit improves read mapping by representing genetic variation in the reference. Nat
514 Biotechnol. Nature Publishing Group; 2018;36:875–9.
515 13. Matsubara D, Kanai Y, Ishikawa S, Ohara S, Yoshimoto T, Sakatani T, et al. Identification
516 of CCDC6-RET Fusion in the Human Lung Adenocarcinoma Cell Line, LC-2/ad. J Thorac
517 Oncol. International Association for the Study of Lung Cancer; 2012;7:1872–6.
518 14. Suzuki A, Makinoshima H, Wakaguri H, Esumi H, Sugano S, Kohno T, et al. Aberrant
519 transcriptional regulations in cancers: Genome, transcriptome and epigenome analysis of lung

520 adenocarcinoma cell lines. Nucleic Acids Res. 2014;42:13557–72.
521 15. Suzuki A, Matsushima K, Makinoshima H, Sugano S, Kohno T, Tsuchihara K, et al. Single-
522 cell analysis of lung adenocarcinoma cell lines reveals diverse expression patterns of individual
523 cells invoked by a molecular target drug treatment. Genome Biol. 2015;16:66.
524 16. Suzuki A, Suzuki M, Mizushima-Sugano J, Frith MC, Makałowski W, Kohno T, et al.
525 Sequencing and phasing cancer mutations in lung cancers using a long-read portable sequencer.
526 DNA Res. 2017;24:585–96.
527 17. Chaisson MJP, Huddleston J, Dennis MY, Sudmant PH, Malig M, Hormozdiari F, et al.
528 Resolving the complexity of the human genome using single-molecule sequencing. Nature.
529 Nature Publishing Group; 2015;517:608–11.
530 18. Sereewattanawoot S, Suzuki A, Seki M, Sakamoto Y, Kohno T, Sugano S, et al.
531 Identification of potential regulatory mutations using multi-omics analysis and haplotyping of
532 lung adenocarcinoma cell lines. Sci Rep. 2018;8:4926.
533 19. Santoro M, Carlomagno F. Central role of RET in thyroid cancer. Cold Spring Harb
534 Perspect Biol. 2013;5:1–17.
535 20. Mizukami T, Shiraishi K, Shimada Y, Ogiwara H, Tsuta K, Ichikawa H, et al. Molecular
536 mechanisms underlying oncogenic RET fusion in lung adenocarcinoma. J Thorac Oncol.
537 International Association for the Study of Lung Cancer; 2014;9:622–30.
538 21. Thorvaldsdóttir H, Robinson JT, Mesirov JP. Integrative Genomics Viewer (IGV): High-
539 performance genomics data visualization and exploration. Brief Bioinform. 2013;14:178–92.
540 22. Munro JE, Dunwoodie SL, Giannoulatou E. SVPV: A structural variant prediction viewer
541 for paired-end sequencing datasets. Bioinformatics. 2017;33:2032–3.
542 23. Wöste M, Dugas M. VIPER: A web application for rapid expert review of variant calls.
543 Bioinformatics. 2018;34:1928–9.

544 24. Kent WJ, Zweig AS, Barber G, Hinrichs AS, Karolchik D. BigWig and BigBed: Enabling
545 browsing of large distributed datasets. Bioinformatics. 2010;26:2204–7.
546 25. Nattestad M, Goodwin S, Ng K, Baslan T, Sedlazeck FJ, Rescheneder P, et al. Complex
547 rearrangements and oncogene amplifications revealed by long-read DNA and RNA sequencing
548 of a breast cancer cell line. Genome Res. 2018;28:1126–35.
549 26. Li H, Durbin R. Fast and accurate short read alignment with Burrows-Wheeler transform.
550 Bioinformatics. 2009;25:1754–60.
551 27. Layer RM, Chiang C, Quinlan AR, Hall IM. LUMPY: a probabilistic framework for
552 structural variant discovery. Genome Biol. 2014;15:R84.
553 28. Rausch T, Zichner T, Schlattl A, Stütz AM, Benes V, Korbel JO. DELLY: Structural variant
554 discovery by integrated paired-end and split-read analysis. Bioinformatics. 2012;28:333–9.
555 29. Chen X, Schulz-Trieglaff O, Shaw R, Barnes B, Schlesinger F, Källberg M, et al. Manta:
556 Rapid detection of structural variants and indels for germline and cancer sequencing
557 applications. Bioinformatics. 2016;32:1220–2.
558 30. Jeffares DC, Jolly C, Hoti M, Speed D, Shaw L, Rallis C, et al. Transient structural
559 variations have strong effects on quantitative traits and reproductive isolation in fission yeast.
560 Nat Commun. 2017;8:1–11.
561 31. Nattestad M, Alford MC, Sedlazeck FJ, Schatz MC. SplitThreader : Exploration and
562 analysis of rearrangements in cancer genomes. bioRxiv. 2016;1–8.
563 32. Jupp S, Malone J, Bolleman J, Brandizi M, Davies M, Garcia L, et al. The EBI RDF
564 platform: Linked open data for the life sciences. Bioinformatics. 2014;30:1338–9.
565 33. Katayama T, Kawashima S, Okamoto S, Moriya Y, Chiba H, Naito Y, et al.
566 TogoGenome/TogoStanza: modularized Semantic Web genome database. Database. 2019;2019.
567 34. Vanderkam D, Aksoy BA, Hodes I, Perrone J, Hammerbacher J. Pileup.js: A JavaScript

568 library for interactive and in-browser visualization of genomic data. Bioinformatics.
569 2016;32:2378–9.
570 35. Suzuki A, Kawano S, Mitsuyama T, Suyama M, Kanai Y, Shirahige K, et al.
571 DBTSS/DBKERO for integrated analysis of transcriptional regulation. Nucleic Acids Res.
572 Oxford University Press; 2018;46:D229–38
573

574 ## ADDITIONAL FILES

575 Additional file 1: Additional figures and tables referenced in the manuscript. (PDF)

576